ARTICLE

Solid phase behavior of mixture systems based on tripalmitoyl glycerol and monounsaturated triacylglycerols forming a molecular compound

Received 00th January 20xx,
Accepted 00th January 20xx

DOI: 10.1039/x0xx00000x

Jorge Macridachis*, Laura Bayés-García and Teresa Calvet

Differential scanning calorimetry and X-ray diffraction were used to investigate the mixing behavior of triacylglycerol (TAG) mixtures of PPP/PPO (tripalmitoyl glycerol/1,2-dipalmitoyl-3-oleoyl-rac-glycerol) and PPP/$MC_{POP/PPO}$ (being $MC_{POP/PPO}$ the equimolecular blend of 1,3-dipalmitoyl-2-oleoyl-glycerol and PPO forming a molecular compound) under metastable and stable conditions. During cooling and reheating treatments at moderate rates, eutectic properties of the two systems examined were mainly governed by the crystallization, transformation, and melting behavior of structurally similar β' forms. In addition, steric and kinetic effects determined the formation of solid solutions with up to 10% and 20% of mixed-acid components in PPP/PPO and PPP/$MC_{POP/PPO}$ mixtures, respectively. These values increased to 30% and 35% when thermodynamically stable β crystalline phases were obtained. In PPP/$MC_{POP/PPO}$ mixtures, diffraction data suggested that POP and PPO acted as a single component by dissolving at a similar amount in solid solution phases and forming molecular compound crystals in eutectic compositions. This fundamental research shows the important role of specific combinations of mixed-acid TAGs and their interaction with high-melting components on the solidification behavior of edible lipids.

1. Introduction

Polymorphic crystallization and mixing phase behavior of lipids play a primary function in the macroscopic properties (melting behavior, texture, plasticity) exhibited by many fat-based food products and in the efficient separation of lipid phases with desired properties during dry fractionation of edible oils.[1] Therefore, the optimal control and design of industrial fat crystallization processes go through an in-depth understanding of the specific molecular interactions that rule the overall behavior of the feedstock. This may become an almost impossible task due to the chemically heterogeneous composition of natural fats, in which triacylglycerols (TAGs) arise as the predominant molecular species. However, reducing the complexity of these systems to binary and ternary mixtures of their major components provides a molecular insight into the principal mixing interactions that define the overall crystallization, melting, and phase transformation behavior.[2,3]
Among typical mixing behavior exhibited by TAGs, structurally similar components may lead to solid solution (ss) formation by exchanging crystallographic positions at all concentration ratios. Full miscibility in the β polymorph was confirmed in the binary system POS/SOS[4] (with S, P, and O being stearic, palmitic, and oleic acid, respectively), which plays a part in the physical properties displayed by cocoa butter. Conversely, TAGs differing in fatty acids length, *sn*- positions, and degree of unsaturation often display eutectic phase behavior. This is typical of fully saturated blends like PPP/PSP or PSP/PPS,[5,6] and oleic-rich binary systems like POP/POO, and PPO/OPO.[7,8] In addition, molecular compounds (MC) with particular structural and thermodynamic properties may occur in certain combinations of mixed-acid components. Specific interactions between functional groups are responsible for the equimolecular compounds with double chain-length structure that form in binary systems such as POP/OPO and POP/PPO.[9]
The research interest in molecular compounds relies on their involvement in diverse edible applications. For example, promoting their formation was suggested as a worthy strategy to increase the thermal stability and solid fat content of lipid systems while reducing their content in *trans* fats.[10] The SR-XRD study carried out on POP/OPO mixtures under kinetic conditions showed that the prevented occurrence of $MC_{POP/OPO}$ during fast cooling processes is minimized by increasing the content ratio of POP, which becomes relevant on the optimal industrial processing of palm- and lard-based margarine.[11,12] Recent work also showed the applicability of molecular compounds in the formulation of cocoa butter equivalents.[13,14]
Despite the above mentioned, the mixing properties of molecular compound-forming TAGs with third components remains largely unexplored. So far, our knowledge on the phase behavior of saturated-unsaturated mixed-acid and fully saturated TAGs is primarily based on two-component mixture systems.[3] These interactions may influence the properties of hard stock blends including oleic acid and the solidification behavior of lipids during fractional crystallization processes. Therefore, determine the effect of different mixed-acid TAG combinations on the phase behavior of blends including high-

Departament de Mineralogia, Petrologia i Geologia Aplicada, Facultat de Ciències de la Terra, Universitat de Barcelona, Martí i Franquès s/n, E-08028 Barcelona, Spain

Please do not adjust margins

melting components becomes a matter of interest. In line with this, a recent study evaluated the mixing properties of PPP and the molecular compound-forming TAGs POP and OPO. It was confirmed that the solid solubility in PPP of the pure mixed-acid components varied depending on whether they were alone or concurrently present at equimolecular ratio in the bulk.[15]

The present work reports on the phase behavior of blends including PPP and the molecular compound-forming TAGs POP and PPO. More specifically, differential scanning calorimetry (DSC) and X-ray diffraction (XRD) techniques, with both laboratory-scale and synchrotron radiation sources, were applied to investigate the thermal and structural properties of PPP/PPO and PPP/$MC_{POP/PPO}$ (with POP and PPO at a 1:1 ratio) mixtures when subjected to a six-month stabilization process and to specific dynamic thermal treatments. Phase diagrams constructed with the resulting experimental data were used to clarify the overall polymorphic crystallization, transformation, and melting behavior of these systems under the different conditions applied. It is worth noting that compared to the extensive research conducted on PPP/POP mixtures under several experimental approaches,[16–19] little data is available on the binary phase behavior of PPP and PPO.[20] Moreover, to the best of our knowledge, no detailed phase behavior studies on ternary mixtures including PPP, POP, and PPO have been carried out yet. A fundamental look into the polymorphism and solid-state miscibility of these systems may help expand the understanding of the mixing interactions that contribute to the crystallization behavior of fats like palm oil, in which the former TAGs represent primary high-melting components.

2. MATERIALS AND METHODS

2.1. Sample preparation

Tripalmitoyl glycerol (PPP), 1,3-dipalmitoyl-2-oleoyl-glycerol (POP), and 1,2-dipalmitoyl-3-oleoyl-rac-glycerol (PPO) (purity ≥ 99%) used in the present study were provided by Larodan AB (Solna, Sweeden) and used without further purification.

To prepare PPP/PPO binary mixtures, molten PPP and PPO were combined at 5-10% molar mass intervals and further homogenized using a vortex mixer. A similar procedure was followed for the ternary mixtures of PPP, POP, and PPO, in which the equimolecular ratio of POP and PPO remained constant to facilitate the solidification of the mixed-acid components in the form of a molecular compound. For this, a 50POP/50PPO stock mixture (to be referred to as $MC_{POP/PPO}$ in this work) was prepared in the first place by melting and blending these TAGs at 50 °C.

To investigate the phase behavior of the PPP/PPO and PPP/$MC_{POP/PPO}$ systems in most stable polymorphs, mixtures in the molten state were first held 5 days at an incubation temperature of 40 °C and then kept for 6 months at 27 °C.

2.2. Differential Scanning Calorimetry (DSC)

The thermal behavior of the mixtures was analyzed using a PerkinElmer DSC-8000 calorimeter. Melting temperature and enthalpy of indium and n-decane standards were used for the calibration of the equipment. An empty pan was used as a reference.

Completely molten samples were weighed (4.0-4.4 mg) into 50 µL aluminum pans and hermetically sealed. The thermal behavior of the mixtures subjected to thermal stabilization was evaluated during a heating treatment from 0 to 80 °C at a rate of 2 °C·min^{-1}. To analyze the miscibility properties of the PPP/PPO and PPP/$MC_{POP/PPO}$ systems in the metastable state, molten mixtures were first cooled to -30 °C and subsequently heated until complete melting. Two different thermal protocols were applied, consisting of 1) cooling and heating at 2 °C·min^{-1}, and b) cooling at 15 °C·min^{-1} and heating at 2 °C·min^{-1}. All experiments were conducted in triplicate.

Onset (T_{onset}), peak top (T_{top}), and end (T_{end}) temperatures (°C), and enthalpy (ΔH, J·g^{-1}) of the main phenomena observed were processed by using Pyris software. A correction described elsewhere[21] was applied to the thermal data obtained at rates different from that used for the equipment calibration (2 °C·min^{-1}). The standard error was calculated by the Student's method approximation to attain a 95% confidence interval. T_{top} values will be used to define the main DSC events detected by DSC in the present study.

2.3. X-ray diffraction experiments

X-ray diffraction experiments with both laboratory-scale and synchrotron radiation (SR) sources were carried out for polymorphic identification of the samples under the same thermal conditions applied by DSC.

A PANalytical X'Pert Pro MPD powder diffractometer operating with Debye-Scherrer transmission geometry and equipped with a hybrid monochromator and a PIXcel detector was used to perform the laboratory-scale XRD measurements. The thermal processing of the samples was carried out with an Oxford Cryostream Plus 220V (temperature 80-500K). In the course of each experiment, a 1 mm diameter Lindemann glass capillary containing the sample was rotated about its axis to minimize preferential crystalline orientation. The step size was 0.013° from 1° to 28° 2θ, and the measuring time 150 s per step.

SR-XRD measurements were carried out at beamline BL11-NCD-SWEET at the ALBA synchrotron (Cerdanyola del Vallès, Barcelona, Spain) at 12.4 keV. The small-angle X-ray diffraction data (SR-SAXD) was collected on a Pilatus 1M detector with a pixel size of 172 X 172 µm^2, whereas a LX255-HS Rayonix detector with a pixel size of 40 X 40 µm^2 was used for the wide-angle scattering (SR-WAXD) data acquisition. During the experiments, the temperature of a 2mm-thick sample contained in an aluminum cell sealed with kaptom film was controlled by a Linkam stage. The q-axis calibration was obtained by measuring silver behenate for SR-SAXD and Cr_2O_3 for SR-WAXD. SR-XRD spectra were acquired at 20 s or 30 s intervals when cooling/heating rates of 15 or 2 °C·min^{-1} were applied, respectively.

This journal is © The Royal Society of Chemistry 20xx

Please do not adjust margins

Please do not adjust margins

3. Results

3.1. Mixing phase behavior of PPP/PPO mixtures

3.1.1. PPP/PPO mixtures subjected to thermodynamic stabilization

The main polymorphic forms identified for the components of the mixtures studied in the present work are shown in Table 1. Figure 1 depicts the diffraction patterns of stabilized PPP/PPO mixtures measured at 10 °C and the DSC thermograms resulting from their heating processing at a rate of 2 °C·min^{-1}. Pure PPP and PPO samples exhibited single DSC peaks ascribed to the melting of their respective most stable polymorph (67.9 and 36.1 °C, respectively). β-2L (PPP) was identified in XRD patterns through the small-angle peak at 4.1 nm and corresponding wide-angle peaks at 0.46, 0.45, 0.40, 0.38, 0.37, and 0.36 nm (denoted by ■). The presence of β'$_1$-3L in the pure PPO sample and the mixtures was recognized through the small-angle peak at 3.3 nm (002 reflection) and wide-angle peaks at 0.44, 0.42, 0.40, and 0.38 nm the wide-angle region.

In mixtures rich in PPP, the monoacid TAG governed the melting behavior until its content declined to 65%. At this composition, the additional presence of β'$_1$-3L (PPO) was confirmed through small-angle reflections at 3.3 and 1.3 nm (005) and a weak endothermic signal detected by DSC at 34 °C. In agreement with previous work on binary mixtures of mixed-acid TAGs,[7,18,22] the occurrence of phase separation in PPP/PPO mixtures is comprehensible by considering that the efficient lateral packing of these TAGs is prevented by steric hindrance between the straight palmitic acid chains of PPP and the bent oleic acid moiety of PPO. In this case, the low molecular compatibility led to a solubility limit of PPO in solid PPP of 35%, a value equivalent to that reported for POP in PPP/POP mixtures evaluated under similar conditions.[15]

Hence, mixtures with a higher amount of PPO were composed of a β-2L solid solution and β'$_1$-3L (PPO), with the latter exhibiting more intense and well-defined DSC and XRD signals as the content of mixed-acid TAG increased in the samples. As illustrated in the phase diagram of Figure 2, PPO showed a steady melting temperature at around 35-36 °C in the mixtures (detailed melting data in given in Table S1 of the ESI†), whereas the liquidus curve defined by solid solution phases rich in PPP towards the PPO sample showed the typical negative slope followed by high-melting components in eutectic systems. In the heating thermograms, the reduction in the peak melting temperature of β-2L at increasing content of molten PPO was accompanied by the ever-decreasing symmetric shape of the corresponding DSC peaks. This behavior continued until the 5PPP/95PPO composition. The weak melting peak of β-2L (T_{top} of 45.4 °C) still detected several degrees above that of β'$_1$-3L (PPO) suggested the presence of a very asymmetric eutectic composition in the PPP/PPO diagram.

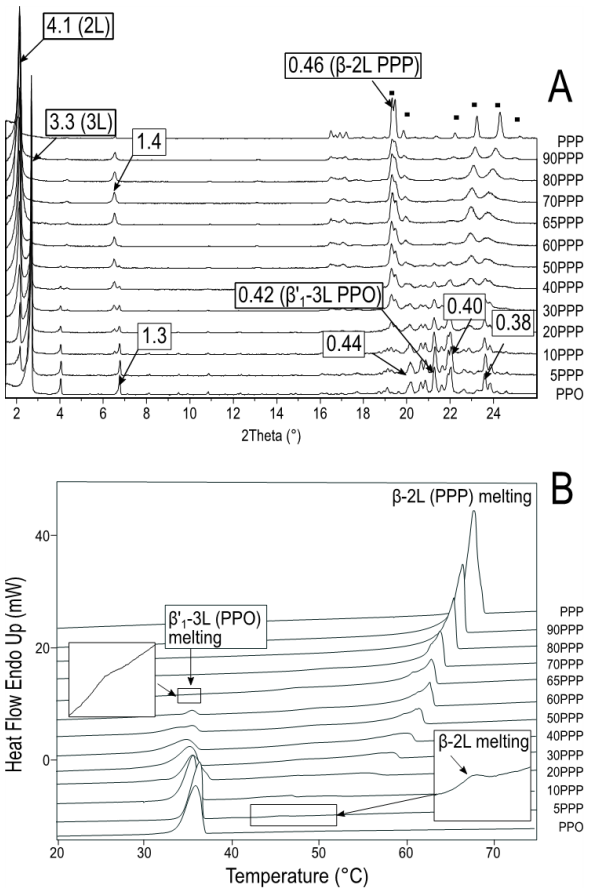

Figure 1. Stabilized PPP/PPO mixtures after kept at 40 °C for 5 days and at 27 °C for 6 months. (A) Laboratory-scale XRD patterns obtained at 10 °C. (B) DSC heating curves at a rate of 2 °C·min^{-1}. ■: β-2L (PPP) wide-angle XRD peaks. *d*-spacing values are given in nm.

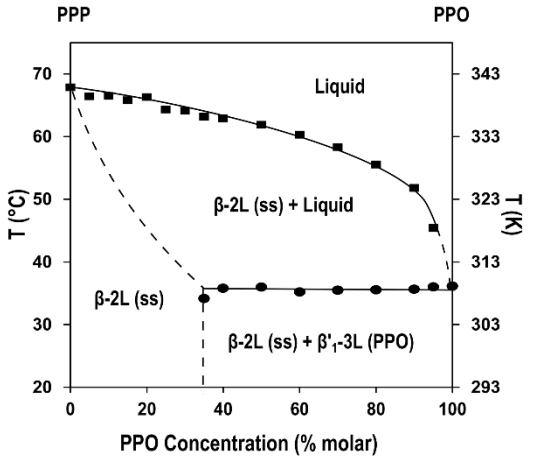

Figure 2. Phase diagram of stabilized PPP/PPO mixtures

Table 1. Long (LS) and short (SS) spacing values of main polymorphic forms identified for of PPP, PPO, and MC$_{POP/PPO}$.

		LS (nm)	SS (nm)
PPP	α-2L	4.5	0.41
	β'-2L	4.2	0.43, 0.42, 0.38
	β-2L	4.1-4.0	0.46, 0.38, 0.37
PPO	α$_2$-2L	4.9 → 4.6	0.41
	α$_1$-3L	3.9 (002)	0.41
	β'$_2$-2L	4.2	0.42, 0.39
	β'$_1$-3L	3.4 (002)	0.42, 0.39
MC$_{POP/PPO}$	α-2L	4.6	0.41, 0.42
	β'-2L	4.3-4.2	0.43, 0.39
	β-2L	4.2	0.46, 0.39, 0.37

→ means a change in *d*-spacing during crystallization

Please do not adjust margins

Please do not adjust margins

3.1.2. PPP/PPO mixtures under kinetic conditions

Understanding the mixing properties of TAGs in their metastable polymorphs is of practical value since obtaining specific forms and preserving their shelf life is aimed in many industrial applications, such as oil fractionation or fat structuring.[23,24] In the present work, the kinetic phase behavior of PPP/PPO mixtures was evaluated during a thermal process consisting of cooling from the melt to -30 °C and next heating at a rate of 2 °C·min^{-1}.

Figure 3 depicts the DSC thermograms obtained for selected mixtures at the above conditions. The exothermic events displayed by the pure PPP sample and the 90PPP/10PPO composition upon cooling were confirmed by XRD (Figures 4A and 4B) as a concurrent crystallization of α-2L (small- and wide-angle peaks at 4.5 and 0.41 nm, respectively) and β'-2L (peaks at 4.2, 0.45, 0.43, 0.42 and 0.38 nm) forms of PPP. When reheating, the melt-mediated α → β' transformation and further β' to β solid transition of pure PPP before melting, in the mixture turned into a single solid-state transformation (DSC exothermic peak at 44.1 °C and occurrence of characteristic β peaks in XRD pattern at 45 °C).

The demixing of TAGs at increasing PPO content resulted in the more complex thermal behavior displayed by the blends with 70, 50, and 30% PPP content in Figure 3. Typical polymorphic behavior is clarified by SR-XRD data of the 50PPP/50PPO composition in Figure 4C. α-2L (PPP) and β'-2L (PPP) crystallized at these compositions on cooling but reflections of the least stable form vanished at decreasing temperature until no α was detected in the samples. The next crystallization of β'$_2$-2L (PPO) (DSC peak at about 20 °C) did not result in evident changes in wide-angle SR-XRD patterns, but the small-angle peak at 4.2 nm increased in intensity and shifted subtly to a lower angle (see amplified image *). In the subsequent heating, β'$_2$-2L (PPO) melted at 30-31 °C without further transformation into the stable β'$_1$-3L (PPO). Its corresponding XRD reflections vanished at around 35 °C (pointed by a white arrow in patterns of the 50PPP/50PPO composition) and those occurring at 0.46, 0.39, and 0.38 nm several degrees above evidenced the next β'-2L (PPP) to β-2L (PPP) transition. According to the endothermic peaks at about 40 °C shown by mixtures with PPP ≤50% before complete melting, a high PPO content favored the occurrence of this transformation through the melt. Despite this, the 50PPP/50PPO composition still showed a weak exothermic signal between β'$_2$-2L (PPO) and β'-2L (PPP) melting (indicated by a white arrow in Figure 3). Since only a decrease in intensity of β' reflections was detected by SR-XRD (see amplified image ** in Figure 4C), this event could be due to the recrystallization of some PPP demixed from the PPO phase after melting or originally present in the mixture in a less stable form.

The increased PPO content in the 10PPP/90PPO composition favored the additional presence of some α$_1$-3L (PPO) at the end of the cooling process. Although very weak, typical small-angle peak at 3.9 nm (002) and wide-angle peak at 0.41 nm were detected in the corresponding XRD patterns (see Figures 4D and 4E). Upon heating, the α$_1$-3L (PPO) → β'$_2$-2L (PPO) transition led to the melt-mediated process observed at around 19 °C in DSC and the vanishing of α diffraction peaks at 25 °C. The following exothermic event at around 26 °C led to a slight shifting of the small-angle reflection of β'$_2$-2L (PPO) towards a higher *d*-spacing (see the enlarged image in Figure 4D). This could be indicative of subtle changes in molecular ordering rather than a polymorphic transformation of PPO. The next endothermic peak at 31 °C corresponded to the sequence of events β'$_2$-2L (PPO) → melt → β'$_1$-3L (PPO) (new small-angle peak with *d*-

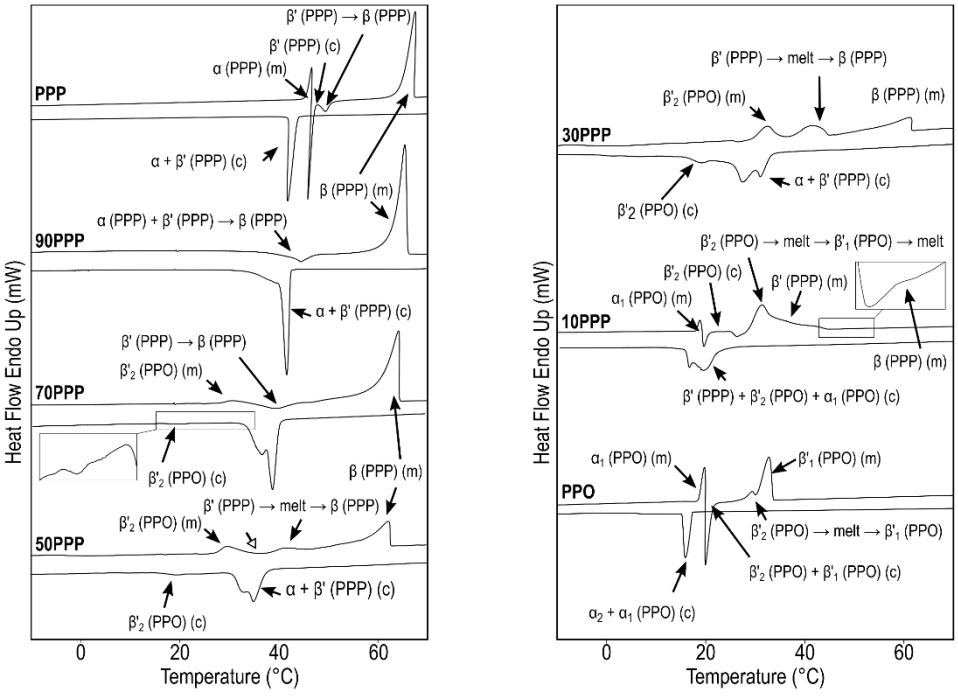

Figure 3. DSC thermograms of PPP/PPO mixtures obtained when cooling and subsequently heating at a rate of 2 °C·min^{-1}. (c): crystallization; (m): melting.

This journal is © The Royal Society of Chemistry 20xx

Please do not adjust margins

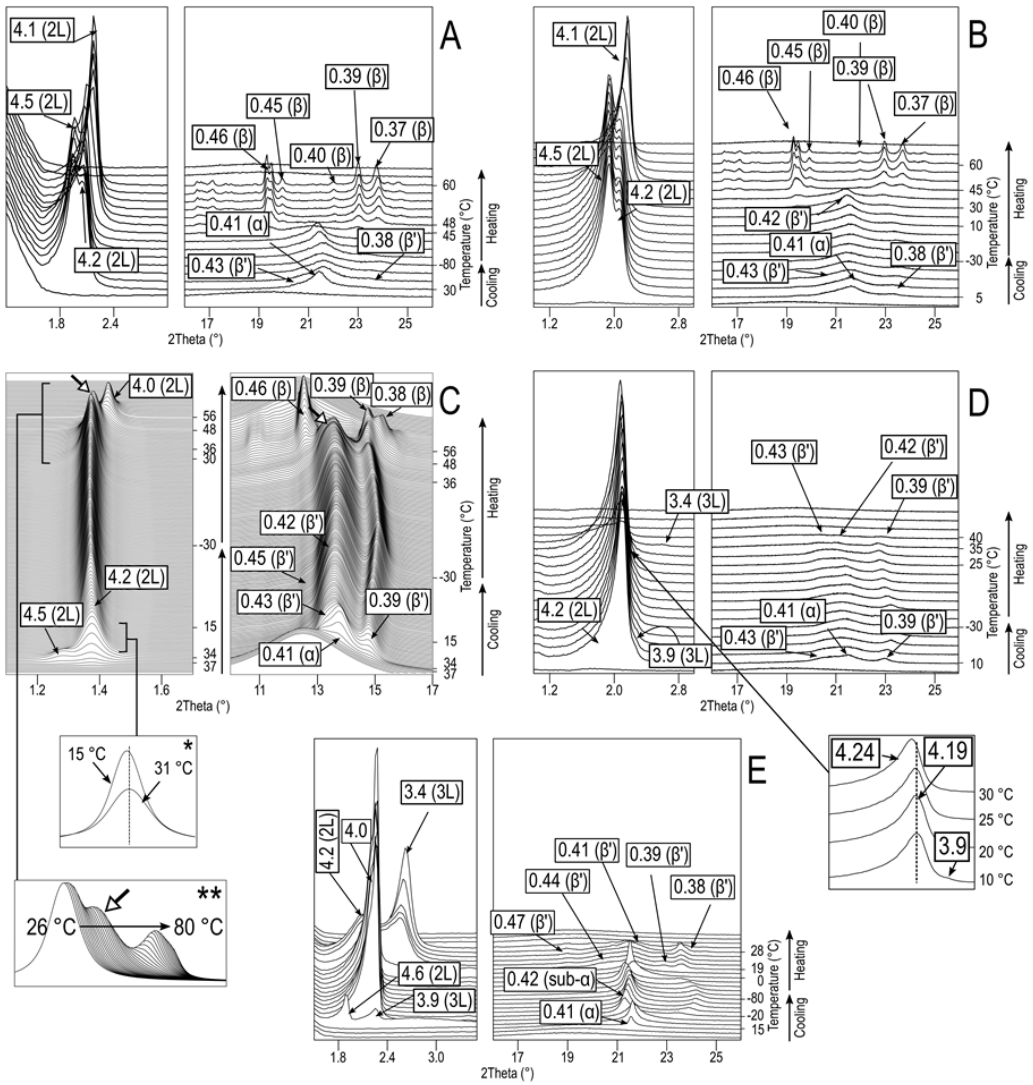

Figure 4. Diffraction data of PPP/PPO mixtures when cooled and subsequently heated at 2 °C·min^{-1}. (A) Pure PPP, (B) 90PPP/10PPO, (C) 50PPP/50PPO, (D) 10PPP/90PPO, and (E) pure PPO. *d*-spacing values are given in nm.

spacing value of 3.4 nm at 35 °C) → melt, after which only β'-2L (PPP) was detected by XRD. Although not properly clarified by XRD data, the last endothermic event detected after β'-2L (PPP) melting suggested that probably some β-2L (PPP) crystals formed before the end of the process.

The polymorphic transformation behavior of PPP/PPO mixtures described above is illustrated in Figure 5 (specific DSC data is included in Table S2 of ESI†). As shown, the occurrence of least stable forms in compositions at the extremes during cooling evidenced the major influence of each TAG on the polymorphic behavior of the mixtures when present at a content above 20%. However, the overall behavior along almost all compositions was governed by the crystallization of eutectic β' phases which showed distinct polymorphic transformation behavior during the heating process. These results contrast with previous data on PPP/PPO mixtures quenched from the melt at 25 °C·min^{-1} to -40 °C and subsequently heated at 5 °C·min^{-1}.[20] Accordingly, sub-α solid solutions were formed in mixtures with PPO above 30%, which during heating sequentially transformed into α and

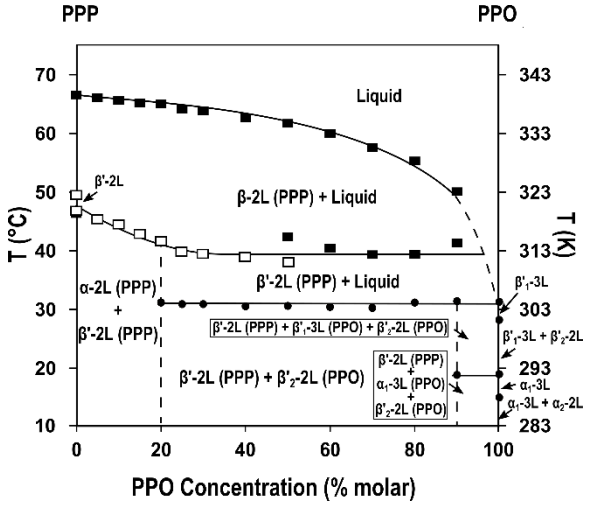

Figure 5. Phase behaviour observed for PPP/PPO mixtures when heating at 2 °C·min^{-1} after a melt crystallization process at the same rate. Delimited areas correspond to polymorphic domains between transitions experimentally determined. Empty symbols: exothermic; filled symbols: endothermic.

Please do not adjust margins

β' solid solutions until phase separation occurred. The divergent behavior of PPP/PPO mixtures in the present study was attributed to the much lower rate applied during the cooling treatment. Previous work underscored how the formation of single phases in lipid systems can be kinetically induced through fast cooling treatments, but phase separation may occur with moderate reductions in the speed of crystallization.[25] Thus, the single α phase obtained during rapid chilling of SSS/PPP mixtures turned into two heterogeneous phases rich in either SSS or PPP when cooling rates below 20 °C·min^{-1} were applied.[26–28] Studies carried out on PPP/POP mixtures also evidenced the effect of faster cooling rates on a poorer separation of TAGs in the metastable state,[16,18,29] which may have implications in the performance of lipid fractionation processes.

In our case, although the structural similarity between β'-2L phases of PPP and PPO complicates the characterization of mixed phases of these components, the clear distinct DSC peaks and the changes in the intensity of XRD signals indicated that one of the β' phases was mainly composed by PPP and the other by PPO. However, strong mixing interactions occurring between PPP and PPO seem responsible for the slight increase in melting temperature undergone by β'_2-2L (PPO), which showed to be above 30 °C in all the mixtures. Furthermore, the closer melting temperature of this form to that of the most stable β'_1-3L (PPO) may be the underlying cause why the occurrence of this form was prevented in mixtures at a PPP content above 10%.

3.2. Mixing phase behavior of PPP/MC$_{POP/PPO}$ mixtures

3.2.1. PPP/MC$_{POP/PPO}$ mixtures subjected to thermodynamic stabilization

Figure 6A depicts laboratory-scale XRD patterns obtained at 10 °C of thermodynamically stabilized PPP/MC$_{POP/PPO}$ mixtures. The presence of PPP in the stable β-2L form could be confirmed by the small-angle peak at 4.1 nm and its characteristic wide-angle XRD peaks (denoted by ■). As for the pure MC$_{POP/PPO}$ mixture, diffraction peaks at 4.2 nm (003 reflection at 1.39 nm) in the small-angle region and 0.46, 0.44, 0.39, and 0.37 nm in the wide-angle region (♦) indicated the occurrence of β-2L (MC$_{POP/PPO}$). In the mixtures, small-angle peaks at 1.36 (003 reflection of peak at 4.1 nm) and 1.39 nm (003 reflection of peak at 4.2 nm) eased the differentiation of the structurally similar β-2L forms of both components when concurrently present.

From pure PPP to the 65PPP/35MC$_{POP/PPO}$ composition, the DSC heating curves obtained at 2 °C·min^{-1} (Figure 6B) showed single endothermic peaks above 60 °C (complete melting data available in Table S3†). This agreed with the sole identification of a β-2L form by XRD. Diffraction peaks associated with the mixed-acid component were not seen in the 60PPP/40MC$_{POP/PPO}$ mixture either. However, the weak endothermic peak observed at 33 °C in its corresponding thermogram long before that attributed to the high-melting TAG was probably due to the β-2L (MC$_{POP/PPO}$) melting. This was supported by the occurrence of endothermic signals at a similar temperature in the mixtures towards pure MC$_{POP/PPO}$. Accordingly, up to 35-40% of MC$_{POP/PPO}$

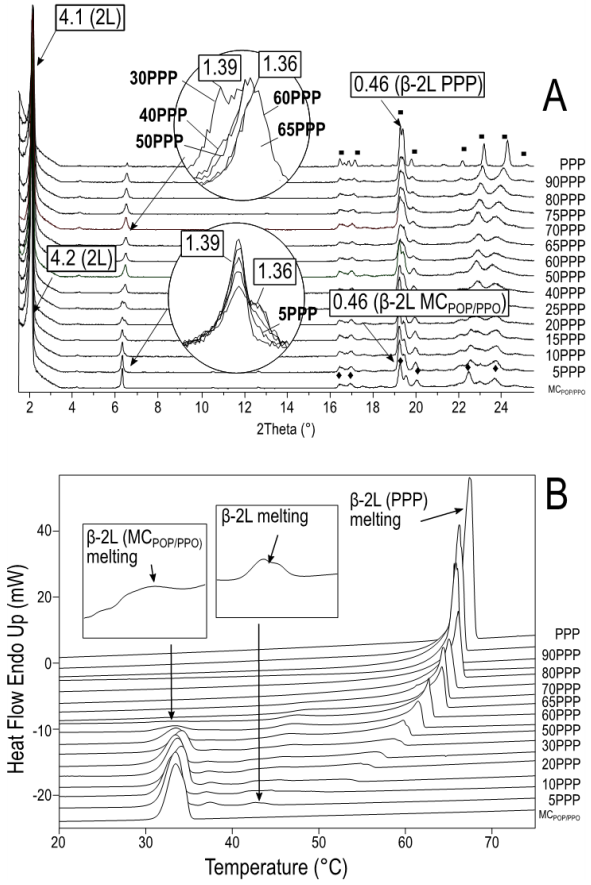

Figure 6. Stabilized PPP/MC$_{POP/PPO}$ mixtures after kept at 40 °C for 5 days and at 27 °C for 6 months. (A) Laboratory-scale XRD patterns obtained at 10 °C. (B) DSC heating curves at a rate of 2 °C·min^{-1}. ■: β-2L (PPP) wide-angle XRD peaks; ♦: β-2L (MC$_{POP/PPO}$) wide-angle XRD peaks. *d*-spacing values are given in nm.

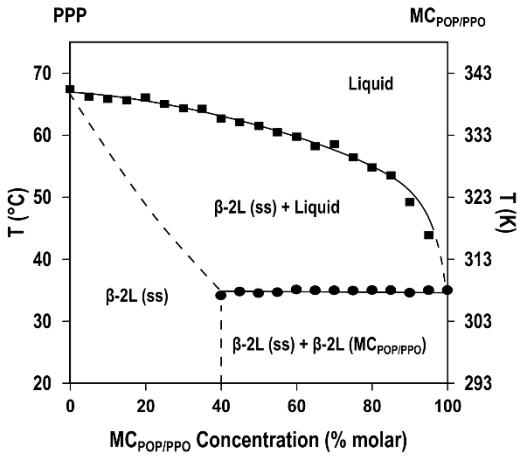

Figure 7. Phase diagram of stabilized PPP/MC$_{POP/PPO}$ mixtures.

was able to solubilize in the solid phase of PPP during thermodynamic stabilization.

Then, the heating curves of mixtures at increasing MC$_{POP/PPO}$ content were characterized by the presence of two main endothermic events corresponding to the successive melting of β-2L (MC$_{POP/PPO}$) and the β-2L phase rich in PPP. The melting of the latter several degrees above β-2L (MC$_{POP/PPO}$) even at the 5PPP/95MC$_{POP/PPO}$ composition, suggested a similar eutectic

 This journal is © The Royal Society of Chemistry 20xx

Please do not adjust margins

Please do not adjust margins

behavior to that ascribed to PPP/PPO and other binary mixtures of TAGs with large differences in melting point. It should be noted that a weak endothermic signal was also detected in the mixtures at around 37 °C, soon after β-2L ($MC_{POP/PPO}$) melting, but no additional small- or wide-angle reflections corresponding to different polymorphic forms were detected for any of the mixtures during the heating treatment (data not shown).

The thermal data obtained during the heating of PPP/$MC_{POP/PPO}$ mixtures at 5% molar mass intervals were used to construct the phase diagram of Figure 7. Overall, the mixing behavior shown by the blends after 6 months of thermodynamic stabilization resembled that observed in the PPP/PPO system. The eutectic region of the diagram showed that POP and PPO behaved as a single component by forming $MC_{POP/PPO}$ in the mixtures. In addition, the absence of experimental signals associated with the presence of pure mixed-acid TAGs in the miscibility region confirmed that neither POP nor PPO was preferentially incorporated in PPP-rich mixed crystals. Probably, the strong molecular interactions associated with the molecular compound formation by these TAGs had a great influence on the final outcome. This would be aligned with the behavior described for other molecular compound-forming TAGs in mixtures with PPP.[15]

3.2.2. PPP/$MC_{POP/PPO}$ mixtures under kinetic conditions

DSC and X-ray diffraction data gathered for selected PPP/$MC_{POP/PPO}$ mixtures during cooling and subsequent heating processes at 2 °C·min^{-1} are depicted in Figures 8 and 9. The thermal data used to illustrate the transformation behavior of crystallized mixtures in Figure 10 is included in Table S4 of ESI†. α-2L (PPP) and β'-2L (PPP) containing small amounts of solubilized mixed-acid TAGs occurred in mixtures with 80% PPP and above during cooling, which in the next heating underwent a solid-solid transformation into β (single exothermic peak at around 40 °C). Below the latter PPP content, mixtures were characterized by the eutectic phases primarily formed by PPP and $MC_{POP/PPO}$ in the metastable state. As in PPP/PPO mixtures, the thermal conditions applied led to a lower miscibility of the components in the metastable state than in the β phases obtained after a thermodynamic stabilization process.

DSC data of mixtures with 70, 50, and 30% PPP content in Figure 8 exemplify the thermal behavior of the system in the eutectic region. SR-XRD data corresponding to the 70PPP/30$MC_{POP/PPO}$ and 50PPP/50$MC_{POP/PPO}$ compositions will be used to clarify the main polymorphic events (Figures 9B and 9C). α-2L (PPP) and β'-2L (PPP) originated from the first convoluted event seen by DSC during cooling. However, α reflections showed a short life in SR-XRD patterns and all PPP was in the form of β' crystals at the end of the process. The second exothermic event occurring near 20 °C was ascribed to the crystallization of β'-2L ($MC_{POP/PPO}$). No changes were detected in wide-angle peaks due to the similar structure of the distinct β' forms, but a strong new signal with a *d*-spacing very close to that of β'-2L (PPP) at 4.2 nm appeared in the small-angle region (see the enlarged image in SR-XRD patterns of the 50PPP/50$MC_{POP/PPO}$ composition). The last crystallization peak near 8 °C was not identified by XRD in mixtures with high PPP content. However, SR-XRD patterns of the 10PPP/90$MC_{POP/PPO}$ composition at around 10 °C (see Figure 9D) showed the occurrence of wide-angle peak at 0.41 nm and small-angle peak at 5.1 nm, which shifted to 4.6 nm on further cooling. This relates to a first separate crystallization of POP and PPO and next formation of α-2L ($MC_{POP/PPO}$).[30,31]

Therefore, it was assumed that the first DSC endothermic peak at around 15 °C in mixtures at 70-30% PPP content during reheating was due to the α-2L ($MC_{POP/PPO}$) melting. The weak thermal signals and the absence of clear diffraction data did not

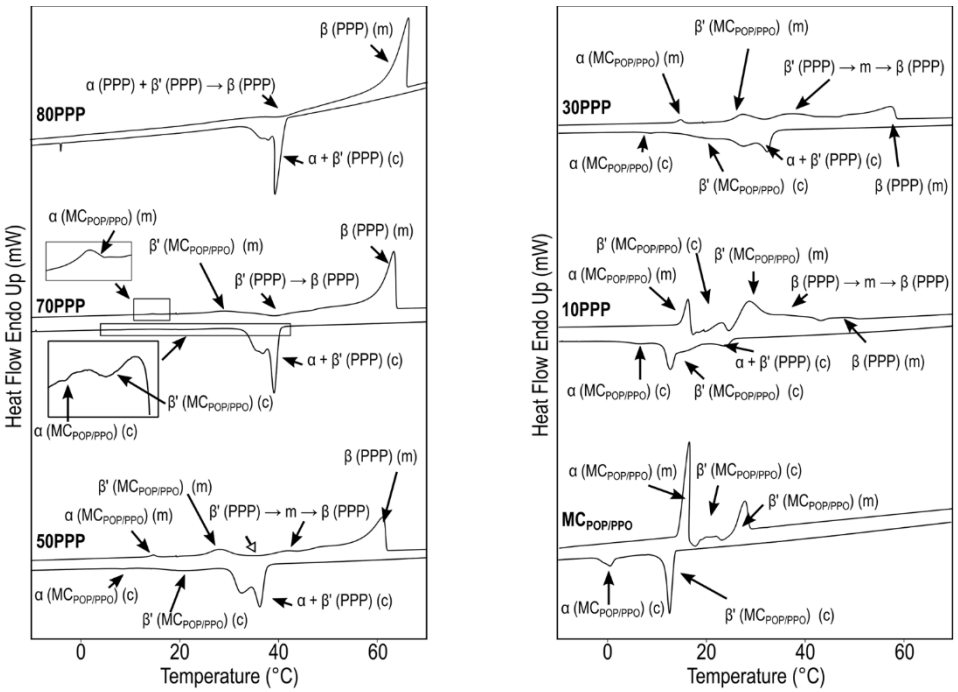

Figure 8. DSC thermograms of selected PPP/$MC_{POP/PPO}$ mixtures when cooling and subsequently heating at a rate of 2 °C·min^{-1}. (c): crystallization; (m): melting.

Please do not adjust margins

Please do not adjust margins

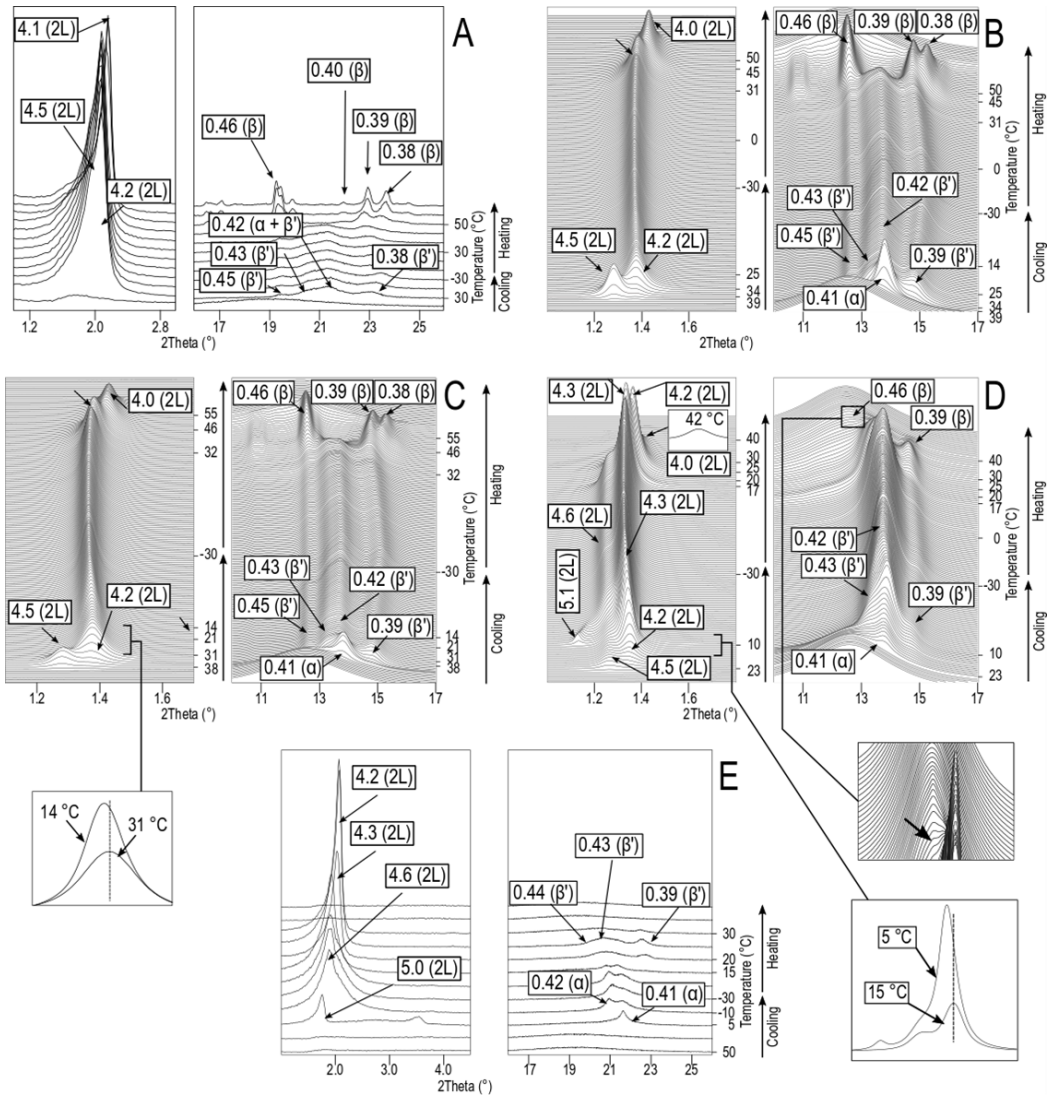

Figure 9. Diffraction data of PPP/$MC_{POP/PPO}$ mixtures obtained when cooled and subsequently heated at 2 °C·min^{-1}. (A) 80PPP/20$MC_{POP/PPO}$, (B) 70PPP/30$MC_{POP/PPO}$, (C) 50PPP/50$MC_{POP/PPO}$, (D) 10PPP/90$MC_{POP/PPO}$, and (E) equimolecular POP/PPO mixture ($MC_{POP/PPO}$). *d*-spacing values are given in nm.

allow to confirm whether or not some additional β'-2L ($MC_{POP/PPO}$) formed next. Afterward, β'-2L ($MC_{POP/PPO}$) melted without further recrystallize in stable β-2L ($MC_{POP/PPO}$) form at any of the compositions. This led to DSC endothermic peaks at around 29 °C and a weakening of β' diffraction peaks due to the only presence of β'-2L (PPP) (pointed by arrows in SR-XRD data of 70PPP/30$MC_{POP/PPO}$ and 50PPP/50$MC_{POP/PPO}$ mixtures). Its corresponding reflections vanished several degrees above and new ones associated with β-2L (PPP) emerged at around 45 °C (wide-angle peaks at 0.46, 0.39, and 0.38 nm), in parallel with the solid-solid transition observed at 39.4 °C in the heating curve of the 70PPP/30$MC_{POP/PPO}$ mixture. The DSC melting peaks of 50PPP/50$MC_{POP/PPO}$ and 30PPP/70$MC_{POP/PPO}$ mixtures at 40 and 37 °C, respectively, evidenced a melt-mediated β' to β transition of PPP in mixtures rich in $MC_{POP/PPO}$. A barely noticeable crystallization peak was still detected in the 50PPP/50$MC_{POP/PPO}$ mixture between β'-2L ($MC_{POP/PPO}$) and β'-2L (PPP) melting (pointed by a white arrow in Figure 8). Although

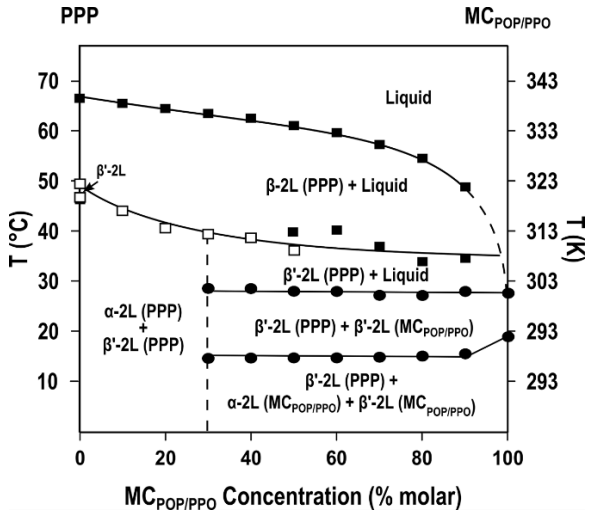

Figure 10. Phase behavior observed for PPP/$MC_{POP/PPO}$ mixtures when heating at 2 °C·min^{-1} after a melt crystallization process at the same rate. Delimited areas correspond to polymorphic domains between transitions experimentally determined. Empty symbols: exothermic; filled symbols: endothermic.

This journal is © The Royal Society of Chemistry 20xx

Please do not adjust margins

Please do not adjust margins

likely related with the transformation of some metastable PPP, its nature could not be clarified by SR-XRD data.

In the 10PPP/90MC$_{POP/PPO}$ mixture, two additional exothermic events occurred after the α-2L (MC$_{POP/PPO}$) melting at around 15 °C. The increase in intensity of the small-angle reflection at 4.3 nm and typical β' wide-angle reflections at 17 °C (Figure 9D) confirmed the first one as the β'-2L (MC$_{POP/PPO}$) recrystallization. The second event (T_{top} of 24.2 °C) corresponded with the shifting of the β'-2L (MC$_{POP/PPO}$) small-angle reflection towards a *d*-spacing value of 4.2 nm, more resembling to that observed for this form in mixtures with higher PPP content. This decrease in *d*-spacing value of β'-2L (MC$_{POP/PPO}$) was also confirmed for the pure MC$_{POP/PPO}$ sample (see XRD data in Figure 9E) and could be attributed to a more compact arrangement of POP and PPO molecules favored during the heating treatment. The subsequent melting of β'-2L (MC$_{POP/PPO}$) at 28 °C was finally followed by the β'-2L (PPP) → β-2L (PPP) transformation (new weak reflections at 4.0 and 0.46 nm when reaching 40 °C) before complete melting.

4. Discussion

The occurrence of complete miscibility, eutectic behavior with partial miscibility, or molecular compound formation in TAG mixtures rely on the effect of aliphatic interactions, methyl-end stacking, and glycerol group's configuration in the stabilization or destabilization of molecular structures.[7,8] As in other eutectic blends containing saturated-unsaturated mixed-acid TAGs,[7,18,22] the difficult lateral packing of components in PPP/PPO and PPP/MC$_{POP/PPO}$ systems under stable and metastable conditions is strongly defined by steric hindrance between palmitoyl and oleoyl chains.

Phase diagrams of PPP/PPO and PPP/MC$_{POP/PPO}$ constructed after 6 months of thermodynamic stabilization showed eutectic points at compositions with PPP content below 5%. The corresponding miscibility regions indicated that 30-35% of PPO and 35-40% of POP/PPO (MC$_{POP/PPO}$) formed solid solution phases with PPP in the β form. Even though the loose molecular packing of α forms may ease total compatibility in some TAG mixtures,[32] the higher density of packing at increasing polymorphic stability restricts complete miscibility in the β form to TAGs with very isomorphic crystal structures. Since eutectic behavior prevails in most TAG mixture systems, defining the extent of partial miscibility regions and the factors involved takes on particular importance in applications addressed to fine-tuning the properties of lipidic materials.

Results obtained in the present work may be better understood if compared with previous data on mixtures of PPP with other molecular-compound forming TAGs.[15] The solubility values determined for pure POP, OPO and their equimolecular mixture in solid PPP under stable conditions are included in Table 2.

Less than 5% OPO dissolved in PPP in the PPP/OPO system, whereas up to 30-35% of pure POP was incorporated in the β crystalline phase of the monoacid TAG. This agrees with the solubility estimated for its asymmetric counterpart PPO in this study. Differences in the magnitude of the disturbing effect of the bent oleic acid chains on the regular zigzag configuration of palmitic acid chains in the PPP crystal lattice could explain the different outcome in these systems.[33] In PPP/OPO mixtures, the resulting excess Gibbs free energy of mixing may be high enough to prevent the formation of PPP/OPO mixed crystals even at a very low content of the diunsaturated TAG. In contrast, the reduced steric hindrance in the binary systems including monounsaturated TAGs may have eased the integration of POP and PPO in solid PPP.

Table 2. Melting point (T_m) and solubility of saturated-unsaturated mixed-acid TAGs in β-2L (PPP) crystals found in the present and previous work.[16]

	Stable form	T_m (°C)	Solubility in PPP
PPP	β-2L	67.9	------
OPO	β_1-3L	22.4	< 5%
POP	β_1-3L	38.0	30-35%
PPO	β'_1-3L	36.1	30-35%
POP/OPO (MC)	β-2L	33.3	20-25%
POP/PPO (MC)	β-2L	33.6	35-40%

The same could explain the different solubility found for the equimolecular blends POP/OPO and POP/PPO despite the similar melting and structural properties of their respective molecular compounds (melting at around 33-34 °C and stable β-2L structures). POP/OPO (MC$_{POP/OPO}$), with a total molar mass of oleic acid in-between that of the component TAGs, displayed a solubility value in PPP (20-25%) considerably higher than OPO but lower than that of POP. The present study showed that introducing an additional palmitic acid chain in the system leads to a higher solubility of POP/PPO (MC$_{POP/PPO}$) in PPP of around 35-40%. One may notice that this value exceeded that shown by its pure TAG components. However, the difference was sufficiently low to consider solubility values of POP, PPO and MC$_{POP/PPO}$ of the same order of magnitude. We may conclude that the miscibility gaps in these systems were primarily defined by the total oleic acid content of the mixed-acid components and a minor or not effect at all is exerted by their symmetry and polymorphic structures under stable conditions.

Binary and ternary mixtures of TAGs rich in palmitic and oleic acid may show complete miscibility in metastable forms after non isothermal crystallization processes at very fast rates.[20] However, phase separation typically occurs along almost the whole range of compositions when moderate-low cooling rates are applied.[18,29] In PPP/PPO mixtures cooled at 2 °C·min^{-1}, α predominated in the pure components at the end of the process but the crystallized mass of the blends was entirely formed by eutectic β' phases. PPP/MC$_{POP/PPO}$ mixtures also showed the promoted occurrence of distinct β' forms, even though some α-2L (MC$_{POP/PPO}$) also occurred at almost all compositions according to DSC data. This behavior relates to actual industrial processes regarding palm oil fractionation, in which the occurrence of large clusters formed by β' crystals is preferred during filtration steps.[34] Although not included in the results section to avoid an extensive length thereof, both mixture systems showed also eutectic behavior in less stable α forms obtained during fast cooling processes at 15 °C·min^{-1} (see experimental data in Figure S1 of ESI†).

Please do not adjust margins

Please do not adjust margins

It has been reported that $MC_{PPP/POP}$, $MC_{POP/PPO}$, and $MC_{PPP/POP/PPO}$ may occur in PPP/POP/PPO mixtures with POO as diluent,[35] although the specifics about structure and stoichiometric properties still need to be clarified in the future. Such behavior could not be confirmed under the experimental conditions used in the present work. Furthermore, the two structurally similar β' phases formed in both PPP/PPO and PPP/$MC_{POP/PPO}$ systems were hardly differentiated even by SR-XRD. Some degree of mutual solubility of components is assumed but the thermal curves obtained during cooling and heating processes suggested that one was mainly formed by mixed-acid TAGs and the other by PPP. In this connection, PPO and POP/PPO ($MC_{POP/PPO}$) showed lower solubility limits in PPP under metastable conditions (10 and 20%, respectively) than in the more densely packed stable β phases. This outcome resulted from the specific thermal treatment applied and shows that a wide range of cooling and heating conditions needs to be tested to clarify the kinetic influence on the mixing properties of TAG systems.

Solidification and mixing properties of TAGs contained in high-melting fractions of complex fats influence the crystallization behavior of lower-melting components. Previous research showed how the seeding effect of PPP in oleic-rich mixtures may be enhanced by formation of mixed crystals of this TAG and POP.[36,37] Our results confirmed similar degree of solid-solubility in PPP/PPO and PPP/POP[15] mixtures under stable conditions. Also, that POP and PPO at equivalent molar mass ratio behaved as a single component when mixed with PPP. $MC_{POP/PPO}$ formed in eutectic compositions and similar amounts of the pure components seemed to incorporate into the solid solution phases. This implies an important role of PPO at the earliest stages of crystallization of fats systems with this TAG as a major component. For example, PPP, POP, and PPO account for approximately 7, 22, and 7% of total TAG content in palm oil.[34] The mixing behavior reported in this study likely contributes to the enrichment in monounsaturated asymmetric TAGs of stearin phases during dry fractionation processes.[24,38]

5. Conclusions

The phase behavior of PPP/PPO and PPP/$MC_{POP/PPO}$ mixtures was evaluated by DSC and X-ray diffraction techniques under stable and metastable conditions. In both systems, melt cooling treatments at 2 °C·min^{-1} favored the formation of eutectic β'-2L forms before the α ones predominantly formed in the pure components. Distinct polymorphic transformation behavior was also monitored during subsequent heating processes at the same rate. High amounts of mixed-acid TAGs prompted melt-mediated β' → β transformations in PPP, whereas small quantities of the latter inhibited the formation of stable β_1'-3L (PPO) crystals in PPP/PPO mixtures. The kinetic influence on the final mixing properties of the systems under study became patent through the lower solubility shown by the mixed-acid components under the mentioned conditions than in the β phases obtained after 6 months of stabilization. From the results obtained for PPP/$MC_{POP/PPO}$ mixtures under stable and kinetic conditions, we concluded similar behavior of POP/PPO to that of a single monounsaturated component. First, POP and PPO showed to be similarly incorporated in the solid solution phases formed with PPP; and second, the total maximum molar solubility of POP/PPO was comparable to that of PPO. In complex lipids, such behavior may contribute to the solidification properties of high-melting components during fractional crystallization.

Conflicts of interest

There are no conflicts to declare.

Acknowledgements

The authors thank financial support through grant MAT2015-65756-R funded by MCIN/ AEI /10.13039/501100011033/ and by "ERDF A way of making Europe", and grant PID-2019-107032RB-I00 funded by MCIN/ AEI /10.13039/501100011033. J. M. was also funded by grant BES-2016-076612 from MCIN/AEI /10.13039/501100011033 and "ESF Investing in your future". Funding from the Alba synchrotron facility for performing SR-XRD experiments is gratefully acknowledged. SR-XRD experiments were conducted with the approval of the Alba Scientific Advisory Committee (proposal 2019023268). The authors thank Dr. Marc Malfois, responsible for BL11-NCD-SWEET at Alba, for his help.

Notes and references

† Electronic supplementary information (ESI) available: DSC data regarding melting and transformation behavior of PPP/PPO and PPP/$MC_{POP/PPO}$ systems (Tables S1-S4). DSC thermograms and SR-XRD patterns obtained for equimolecular PPP/PPO and PPP/$MC_{POP/PPO}$ mixtures during a thermal treatment consisting of cooling rate of 15 °C·min^{-1} and subsequent heating at 2 °C·min^{-1} (Figure S1).

1 K. Sato, Crystallization behaviour of fats and lipids — a review, *Chem. Eng. Sci.*, 2001, **56**, 2255–2265.

2 L. Zhang, S. Ueno and K. Sato, Binary phase behavior of saturated-unsaturated mixed-acid triacylglycerols—A review, *J. Oleo Sci.*, 2018, **67**, 679–687.

3 J. Macridachis-González, L. Bayés-García and T. Calvet, An insight into the solid-state miscibility of triacylglycerol crystals, *Molecules*, 2020, **25**, 4562.

4 P. Rousset, M. Rappaz and E. Minner, Polymorphism and solidification kinetics of the binary system POS-SOS, *J. Am. Oil Chem. Soc.*, 1998, **75**, 857–864.

5 M. Knoester, P. De Bruijne and M. van Den Tempel, The solid-liquid equilibrium of binary mixtures of triglycerides with palmitic and stearic chains, *Chem. Phys. Lipids*, 1972, **9**, 309–319.

6 K. Bhaggan, K. W. Smith, C. Blecker and S. Danthine, Binary mixtures of tripalmitoylglycerol (PPP) and 1,3-dipalmitoyl-2-stearoyl-sn-glycerol (PSP): Polymorphism and kinetic phase behavior, *Eur. J. Lipid Sci. Technol.*, 2018, **120**, 1700306.

This journal is © The Royal Society of Chemistry 20xx

Please do not adjust margins

Please do not adjust margins

7 L. Zhang, S. Ueno, S. Miura and K. Sato, Binary phase behavior of 1,3-dipalmitoyl-2-oleoyl-sn-glycerol and 1,2-dioleoyl-3-palmitoyl-rac-glycerol, *J. Am. Oil Chem. Soc.*, 2007, **84**, 219–227.

8 L. Bayés-García, T. Calvet, M. À. Cuevas-Diarte, S. Ueno and K. Sato, Phase behavior of binary mixture systems of saturated-unsaturated mixed-acid triacylglycerols: Effects of glycerol structures and chain-chain interactions, *J. Phys. Chem. B*, 2015, **119**, 4417–4427.

9 A. Minato, J. Yano, S. Ueno, K. Smith and K. Sato, FT-IR study on microscopic structures and conformations of POP-PPO and POP-OPO molecular compounds, *Chem. Phys. Lipids*, 1997, **88**, 63–71.

10 A. N. Sibbald, J. R. Carney and A. G. Marangoni, Enhanced structuring of fat with reduced saturates using mixed molecular compounds, *J. Am. Oil Chem. Soc.*, 2016, **93**, 1441–1452.

11 K. Nakanishi, Y. Mikiya, T. Ishiguro and S. Ueno, Crystallization behavior of molecular compound in binary mixture system of 1,3-dioleoyl-2-palmitoyl-sn-glycerol and 1,3-dipalmitoyl-2-oleoyl-sn-glycerol, *J. Am. Oil Chem. Soc.*, 2018, **95**, 51–59.

12 K. Nakanishi and S. Ueno, Mixing ratio and cooling rate dependence of molecular compound formation in OPO/POP binary mixture, *Molecules*, 2020, **25**, 5253.

13 S. Watanabe, S. Yoshikawa, T. Arishima and K. Sato, Polymorphism and mixing phase behavior in ternary mixture systems of SOS-SSO-OSO: formation of molecular compound crystals, *J. Am. Oil Chem. Soc.*, 2018, **95**, 447–460.

14 S. Watanabe, S. Yoshikawa and K. Sato, Formation and properties of dark chocolate prepared using fat mixtures of cocoa butter and symmetric/asymmetric stearic-oleic mixed-acid triacylglycerols: Impact of molecular compound crystals, *Food Chem.*, 2021, **339**, 127808.

15 J. Macridachis, L. Bayés-García and T. Calvet, Mixing phase behavior of tripalmitin and oleic-rich molecular compound-forming triacylglycerols, *Ind. Eng. Chem. Res.*, 2021, **60**, 5374–5384.

16 V. Gibon, F. Durant and C. Deroanne, Polymorphism and intersolubility of some palmitic, stearic and oleic triglycerides: PPP, PSP and POP, *J. Am. Oil Chem. Soc.*, 1986, **63**, 1047–1055.

17 K. Kerridge, Melting-point diagrams for binary triglyceride systems, *J. Chem. Soc.*, 1952, 4577–4579.

18 A. Minato, S. Ueno, J. Yano, Z. H. Wang, H. Seto, Y. Amemiya and K. Sato, Synchrotron radiation X-ray diffraction study on phase behavior of PPP-POP binary mixtures, *J. Am. Oil Chem. Soc.*, 1996, **73**, 1567–1572.

19 K. W. Smith, F. W. Cain and G. Talbot, Crystallisation of 1,3-dipalmitoyl-2-oleoylglycerol and tripalmitoylglycerol and their mixtures from acetone, *Eur. J. Lipid Sci. Technol.*, 2005, **107**, 583–593.

20 V. Gibon and F. Durant, Etude du polymorphisme et de l'intersolubilite de triglycerides palmito-oleiques par diffraction rx de poudres et analyse calorimetrique differentielle, *Bull. des Sociétés Chim. Belges*, 1985, **94**, 1009–1020.

21 PerkinElmer, *Instructions Model DSC-4*, Norwalk, Connecticut, USA, 1982.

22 L. Zhang, S. Ueno, K. Sato, R. O. Adlof and G. R. List, Thermal and structural properties of binary mixtures of 1,3-distearoyl-2-oleoyl-glycerol (SOS) and 1,2-dioleoyl-3-stearoyl-sn-glycerol (sn-OOS), *J. Therm. Anal. Calorim.*, 2009, **98**, 105–111.

23 S. Yoshikawa, S. Watanabe, Y. Yamamoto and F. Kaneko, Binary phase behavior of 1,3-distearoyl-2-oleoyl-sn-glycerol (SOS) and trilaurin (LLL), *Molecules*, 2020, **25**, 5313.

24 K. W. Smith, in *Crystallization processes in fats and lipid systems*, eds. N. Garti and K. Sato, Marcel Dekker, New York, NY, USA, 2001, pp. 357–380.

25 J. H. Los, W. J. P. van Enckevort, E. Vlieg, E. Flöter and F. G. Gandolfo, Metastable states in multicomponent liquid-solid systems II : Kinetic phase separation, *J. Phys. Chem. B*, 2002, **106**, 7331–7339.

26 E. S. Lutton, Phase behavior of triglyceride mixtures involving primarily tristearin, 2-oleyldistearin, and triolein, *J. Am. Oil Chem. Soc.*, 1955, **32**, 49–53.

27 W. MacNaughtan, I. A. Farhat and C. Himawan, A differential scanning calorimetry study of the crystallization kinetics of tristearin-tripalmitin mixtures, *J. Am. Oil Chem. Soc.*, 2006, **83**, 1–9.

28 C. Himawan, W. MacNaughtan, I. A. Farhat and A. G. F. Stapley, Polymorphic occurrence and crystallization rates of tristearin/tripalmitin mixtures under non-isothermal conditions, *Eur. J. Lipid Sci. Technol.*, 2007, **109**, 49–60.

29 C. Lu, B. Zhang, H. Zhang, Y. Guo, L. Dang, Z. Liu, Q. Shu and Z. Wang, Solid–liquid phase equilibrium and phase behaviors for binary mixtures composed of tripalmitoylglycerol (PPP), 1,3-dipalmitoyl-2-oleoyl-glycerol (POP), and 1,2-dioleoyl-3-palmitoyl-glycerol (POO), *Ind. Eng. Chem. Res.*, 2019, **58**, 10044–10052.

30 A. Minato, S. Ueno, K. Smith, Y. Amemiya and K. Sato, Thermodynamic and kinetic study on phase behavior of binary mixtures of POP and PPO forming molecular compound systems, *J. Phys. Chem. B*, 1997, **101**, 3498–3505.

31 K. Taguchi, A. Toda, H. Hondoh, S. Ueno and K. Sato, Kinetic study on alpha-form crystallization of mixed-acid triacylglycerols POP, PPO, and their mixture, *Molecules*, 2021, **26**, 220.

32 M. Takeuchi, S. Ueno and K. Sato, Synchrotron radiation SAXS/WAXS study of polymorph-dependent phase behavior of binary mixtures of saturated monoacid triacylglycerols, *Cryst. Growth Des.*, 2003, **3**, 369–374.

33 L. H. Wesdorp, J. A. Van Meeteren, S. de Jong, R. van der Giessen, P. Overbosch, P. A. M. Grootscholten, M. Struik, E. Royers, A. Don, T. de Loos, C. Peters and I. Gandasasmita, in *Structure and properties of fat crystal networks*, eds. A. G. Marangoni and L. H. Wesdorp, CRC Press, Boca Raton, FL, USA, 2nd edn., 2013, pp. 241–418.

34 Y. Basiron, in *Bailey's industrial oil and fat products*, ed. F. Shahidi, John Wiley & Sons, Hoboken, NJ, USA, sixth., 2005,

Please do not adjust margins

Please do not adjust margins

pp. 333–429.
35 R. West and D. Rousseau, Tripalmitin-driven crystallization of palm oil: The role of shear and dispersed particles, *J. Am. Oil Chem. Soc.*, 2020, **97**, 989–999.
36 J. Vereecken, V. de Graef, K. W. Smith, J. Wouters and K. Dewettinck, Effect of TAG composition on the crystallization behaviour of model fat blends with the same saturated fat content, *Food Res. Int.*, 2010, **43**, 2057–2067.
37 J. Vereecken, I. Foubert, K. W. Smith and K. Dewettinck, Effect of SatSatSat and SatOSat on crystallization of model fat blends, *Eur. J. Lipid Sci. Technol.*, 2009, **111**, 243–258.
38 E. Deffense, Fractionation of palm oil, *J. Am. Oil Chem. Soc.*, 1985, **62**, 376–385.

This journal is © The Royal Society of Chemistry 20xx

Please do not adjust margins